1.E.4:2.H Nuclear Physics A194 (1972) 113—139; © North-Holland Publishing Co., Amsterdam

GAMMA DECAY OF LOW-LYING STATES NEAR THE ^{208}Pb CLOSED SHELL

O. HÄUSSER, F. C. KHANNA and D. WARD
Physics Division, Chalk River Nuclear Laboratories, Atomic Energy of Canada Limited, Chalk River, Ontario, Canada

Received 16 May 1972

Abstract: A number of electromagnetic matrix elements between low-lying states of several nuclei near ^{208}Pb have been measured. Coulomb excitation of states in ^{204,206,207,208}Pb and ^{209}Bi has been studied with beams of ^{4}He and ^{16}O. The energy loss of ^{4}He and ^{16}O in Pb has been measured by a novel method and thus accurate B(E2) and B(E3) values were obtained. Gamma-ray lineshapes observed after ^{16}O bombardment were used to derive mean lifetimes of states at 2646.5 keV ($\tau = 0.125 \pm 0.030$ ps) in ^{206}Pb, and at 897.7 keV ($\tau = 0.19 \pm 0.04$ ps), at 2624.4 keV ($\tau = 0.13 \pm 0.05$ ps), and at 2662.4 keV ($\tau = 0.95 \pm 0.20$ ps) in ^{207}Pb. The reactions ^{208}Pb(^{7}Li, $\alpha 2n\gamma$)^{209}Bi and ^{208}Pb(^{7}Li, ^{6}Liγ)^{209}Pb were used for the first time to derive several lifetimes and branching ratios in ^{209}Bi and ^{209}Pb. An intermediate-coupling calculation has been performed which reproduces extremely well the known B(E2) values in ^{207,208}Pb and ^{209}Bi and which qualitatively explains the observed E1 matrix elements. Evidence for retardation of single-particle M1 transitions is presented. The main cause for the retardation is excitations of spin-orbit partners. Possible contributions from higher-order excitations and from mesonic exchange currents are discussed.

E | NUCLEAR REACTIONS ^{204,206,207,208}Pb, ^{209}Bi(α, $\alpha'\gamma$), E = 15–18 MeV; ^{204,206,207,208}Pb, ^{209}Bi(^{16}O, ^{16}O$'\gamma$), E = 69–80 MeV; measured E_γ, $\sigma(E_\gamma)$, DSA. ^{208}Pb(^{7}Li, $\alpha 2n\gamma$)^{209}Bi, ^{208}Pb(^{7}Li, ^{6}Liγ)^{209}Pb, E = 28–31.5 MeV; measured $\alpha\gamma$-coin, E_γ, DSA. ^{204,206,207,208,209}Pb, ^{209}Bi deduced B(Eλ), B(Mλ) and lifetimes. Enriched and natural targets. Measured dE/dx of α and ^{16}O in natural Pb between E_α = 10–18 MeV, $E_{^{16}\mathrm{O}}$ = 28–72 MeV.

1. Introduction

The low-energy states of mass-209 (207) nuclei can be described as either single-particle (hole) states, or as single-particle (hole) states coupled to collective modes of excitation of the ^{208}Pb core. It is currently believed [1-10]) that fractions of the single-particle strengths are found in the collective states, and vice versa, as a result of particle-vibration coupling. Evidence for this fractionation has come to a large extent from nucleon-transfer reactions [1,3-7]). Since standard DWBA analysis does not allow the extraction of accurate spectroscopic factors, particularly for weak transitions [11]), measurements of electromagnetic (EM) matrix elements are useful to complement the available information from nucleon-transfer reactions.

A large part of the present information on EM properties of states near ^{208}Pb comes from inelastic electron scattering [12]), Coulomb excitation [8-10,13,14]) and direct decay time [15-17]) experiments. The early work on Coulomb excitation [13,14]) was severely limited by the poor resolution of NaI(Tl) detectors. The resulting uncertainties in $B(E\lambda)$ values did not allow detailed comparisons with the predictions of the intermediate-coupling model to be made. In the first experimental part (sect. 2) of the present work we report results on Coulomb excitation of low-lying states in $^{204,206-208}$Pb and in ^{209}Bi using beams of ^{4}He between 15 and 18 MeV and beams of ^{16}O between 69 and 80 MeV. First accounts of this work have appeared in laboratory reports [18]) and in a compilation [19]). After completion of these experiments the work of the Heidelberg group [10]) was published which has a large overlap with our study of the Pb isotopes. There are however a number of differences which make a brief description of our experimental methods necessary. A novel technique will be described which was used to measure the energy loss, dE/dx, of ^{4}He and ^{16}O in Pb. We have used these data instead of sometimes unreliable semi-empirical extrapolations for dE/dx to deduce absolute cross sections and $B(E\lambda)$ values with an accuracy approaching ± 5 %. The Doppler-broadened γ-ray lines observed in Ge(Li) detectors after ^{16}O bombardment were interpreted by the Doppler-shift attenuation method (DSAM) to obtain lifetime information. An exact method of calculating unattenuated lineshapes at arbitrary observation angles is described. Reasonable assumptions for the slowing down of the recoils are then introduced to relate the observed distortion and shift of the unattenuated lineshape to the lifetime of the initial state.

In a second experimental part (sect. 3), the ^{7}Li-induced reactions ^{208}Pb(^{7}Li, ^{6}Li γ) ^{209}Pb and ^{208}Pb(^{7}Li, $\alpha 2n\gamma$)^{209}Bi were used to study the γ-decay of the $1i_{\frac{11}{2}}$ and $3d_{\frac{5}{2}}$ single-neutron states in ^{209}Pb and the $2f_{\frac{7}{2}}$ and $3p_{\frac{3}{2}}$ single-proton states in ^{209}Bi. The latter reaction provided also data on lifetimes and branching ratios for the $(1h_{\frac{9}{2}} \otimes 3^-)$ septuplet of states near 2.6 MeV which had been measured previously [8,9]).

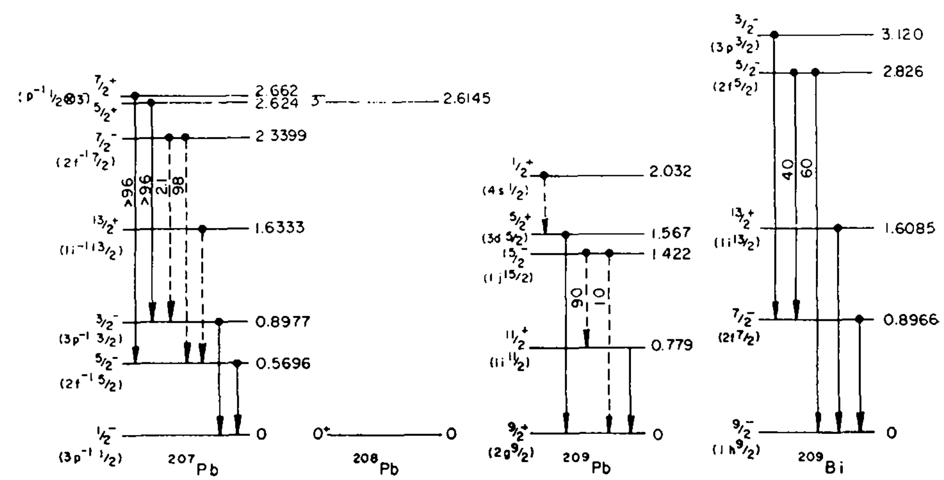

Fig. 1. Decay scheme of some low-lying states discussed in the present work. The $(h_{\frac{9}{2}} \otimes 3^-)$ septuplet near 2.6 MeV in ^{209}Bi has been omitted.

In fig. 1 some of the states studied in the present work are shown with their main configurations, excitation energies, and γ-decay modes. It is seen that a fairly large number of E1, E2 and E3 matrix elements are now available in mass-207 and mass-209 nuclei, particularly if we also consider the ^{209}Bi septuplet (not shown in fig. 1). Intermediate-coupling calculations have been performed (sect. 4) starting from specific collective phonon states J in the ^{208}Pb core and from experimental values for $B(\mathrm{E}\lambda;\ \mathrm{g.s.} \to J)$. The purpose of these calculations is to investigate whether the same intermediate-coupling parameters can explain the data in the three nuclei ^{207}Pb, ^{209}Pb and ^{209}Bi.

Several M1 matrix elements are now known in mass-207 and mass-209 nuclei from direct lifetime measurements or can be inferred from measurements of mixing ratios, branching ratios and $B(\mathrm{E}\lambda)$ values. The three l-allowed M1 transitions between single-particle (hole) states known so far in ^{207}Pb and ^{209}Bi are inhibited by at least a factor of two. Deviations of magnetic moments from the Schmidt value are of course familiar and result mainly [20, 21]) from excitations of $1i_{\frac{13}{2}} \to 1i_{\frac{11}{2}}$ (neutron) and $1h_{\frac{11}{2}} \to 1h_{\frac{9}{2}}$ (proton). In addition to the renormalization of the one-body operator there are two-body contributions to M1 matrix elements originating from mesonic exchange currents between any two nucleons. Calculations by Chemtob [22]) showed that two-body terms contribute significantly to the anomalous magnetic moment of ^{209}Bi(g.s). In sect. 5 the relative importance of one- and two-body renormalization of M1 matrix elements will be briefly discussed. A more detailed account of this work will be published elsewhere [23]).

2. Coulomb excitation of $^{204,\,206-208}$Pb and ^{209}Bi

2.1. EXPERIMENTAL METHOD

The experiments were performed with the $^{4}\mathrm{He}^{2+}$, $^{16}\mathrm{O}^{6+}$ and $^{16}\mathrm{O}^{7+}$ beams from the Chalk River MP tandem accelerator at bombarding energies of 15, 16.5, 17 and 18 MeV for ^{4}He and of 69, 70, 77 and 80 MeV for ^{16}O. About 400 mg/cm^2 thick rolled targets of natural Pb and Bi, and of isotopically enriched ^{206}Pb (99.8 %), ^{207}Pb(92.4 %) and ^{208}Pb(96.0 %) were used. The experimental arrangement used for thick-target yield measurements has been described in detail previously [24, 25]). The target chamber is insulated from the beam transport system by a glass tube and serves as a Faraday cup. A suppression electrode at $-$ 2 kV prevents secondary electrons from entering or leaving the Faraday cup. A pressure of $< 10^{-7}$ Torr was maintained between the last quadrupole magnet and target to avoid charge exchange of the heavy-ion beams.

De-excitation γ-rays were observed at several angles between 0° and 110° with respect to the beam direction in two 45 cm^3 Ge(Li) detectors with a resolution of 2.3 keV at 1 MeV. The gain and cut of one of the detector systems was stabilized with a method described by Broude [26]). For this purpose two peaks from 60 Hz precision pulsers were gated into the very low- and the very high-energy ends of one of the spec-

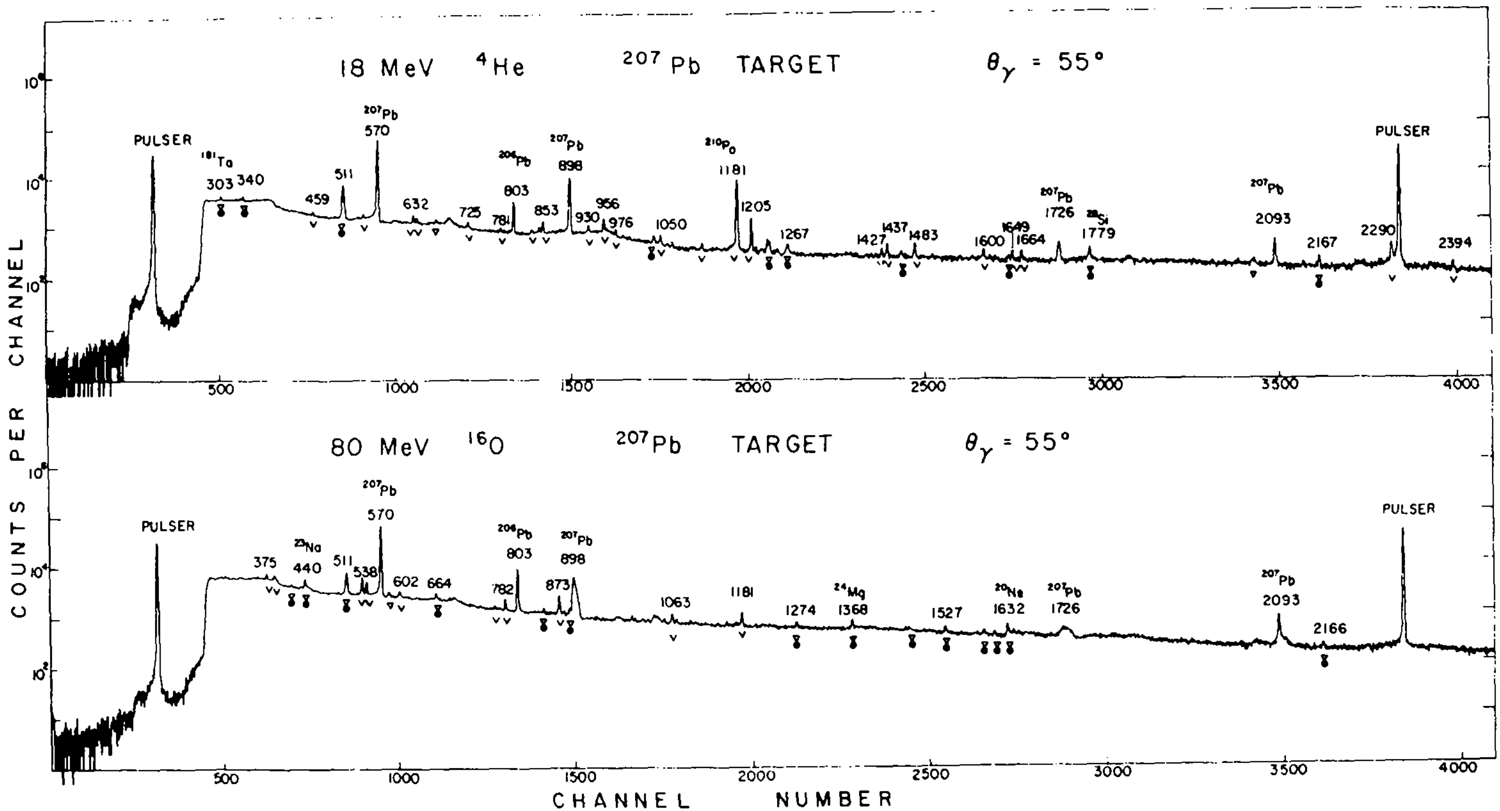

Fig. 2. Singles γ-spectra obtained at $\theta_\gamma = 55°$ after bombardment of a ^{207}Pb target with 18 MeV ^{4}He and 80 MeV ^{16}O.

tra to derive on-line corrections for the relevant encoder. Two of the stabilized spectra observed at $\theta_\gamma = 55°$ using 18 MeV ^{4}He and 80 MeV ^{16}O beams and a ^{207}Pb target are shown in fig. 2. The lines with unshifted energies of 570, 898, 1726 and 2093 keV result from Coulomb excitation of ^{207}Pb, whereas the 803 keV line comes from a small fraction of ^{206}Pb in the target. In addition to these lines a large number of other γ-rays are present. Some of these lines (marked v) disappear rapidly at lower bombarding energies. The most prominent of these is the 1181 keV line in the upper spectrum originating from the first excited state of ^{210}Po after the ^{207}Pb(α, n)^{210}Po reaction [27]. Other lines appear also at lower bombarding energies ($\triangledown$) or with all other targets ($\bullet$) or both, and result most likely from light contaminants. The lines from (heavy-ion, xn) reactions are found to be large at energies above 17 MeV ^{4}He and 70 MeV ^{16}O indicating that nuclear interactions have to be taken into account in this energy region. Similar conclusions were obtained from excitation functions (see below) and from elastic scattering measurements [28].

Energies of γ-ray lines were obtained from spectra which contained, in addition to ^{4}He data at $\theta_\gamma = 90°$, lines from several radioactive sources covering the energy region between 511 keV (from ^{22}Na) and 1836.1 keV (from ^{88}Y). The efficiency of the detectors was obtained from calibrated radioactive sources † placed at the beam spot on the target. Corrections for measured electronic dead-time losses were applied to all data.

2.2. ENERGY-LOSS MEASUREMENTS

In this section a novel method is described of measuring the energy loss, dE/dx, of heavy ions in solids. The energy loss, 10–18 MeV ^{4}He and 25–80 MeV ^{16}O in Pb, is required to deduce absolute cross sections from the measured γ-ray yields. These data were not available and semi-empirical extrapolations [29–31] predict different values.

A 1.5 mg/cm^2 layer of natural lead was evaporated onto a 10 μg/cm^2 carrier foil of cellulose nitrate. One half of the foil was masked during the evaporation of lead. Onto both halves a 30 μg/cm^2 surface layer of copper was evaporated to prevent oxidation of the Pb surface. The three-layer foil was mounted in front of a surface-barrier detector with the lead boundary parallel to the scattering plane of an Ortec scattering chamber. Particles of ^{4}He and ^{16}O of the required energy were produced by elastic scattering of small-intensity beams from $\approx$ 50 μg/cm^2 self-supporting lead foils. Two clearly resolved peaks were observed in the surface-barrier detector. The difference of the peak centroids is proportional to the effective dE/dx in the lead. Finally, the thickness of the lead in the three-layer foil was determined by Rutherford scattering of a 13 MeV ^{4}He^{2+} beam. The uniformity of the deposit, tested by moving the target, was better than 1.5 %.

The results are shown in fig. 3 together with semi-empirical extrapolations according to Northcliffe and Schilling [29]) (solid lines), Williamson *et al.* [30] (dashed line,

† Supplied by International Atomic Energy Agency, Vienna.

^{4}He), and Booth and Grant [31]) (dashed line, ^{16}O). The systematic errors in the measured dE/dx were estimated to be < 2.5 %. Both the ^{4}He and ^{16}O data are in good agreement with the predictions of Northcliffe and Schilling [29]). The Booth and Grant parametrization of the ^{16}O effective charge, used in the Coulomb excitation work of ref. [10]), overestimates dE/dx by typically 10 %.

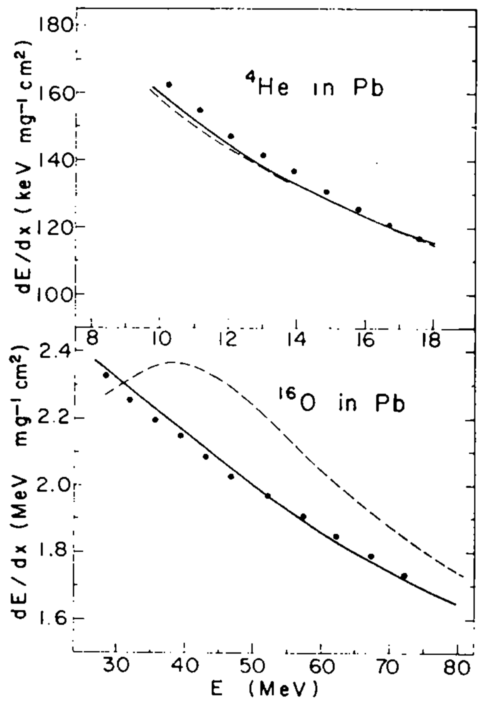

Fig. 3. Energy loss of ^{4}He and ^{16}O ions in natural Pb. The solid lines are extrapolated values from the compilation of Northcliffe and Schilling [29]). The dashed lines are taken from ref. [30]) for ^{4}He ions and are calculated with the semi-empirical formulae of ref. [31]) for ^{16}O ions.

2.3. THE B(Eλ) VALUES AND STATIC QUADRUPOLE MOMENTS

The measured γ-ray yields were compared with theoretical Coulomb excitation calculations to deduce B(Eλ) values and, possibly, static quadrupole moments Q_s of the octupole vibrational states. The Winther-de Boer Coulomb excitation program [32]) was used to calculate excitation cross sections and γ-ray angular distributions for a given set of B(Eλ), Q_s, scattering angle and bombarding energy. To obtain thick-target yields the cross sections were weighted by the experimental $(\mathrm{d}E/\mathrm{d}x)^{-1}$ and integrated over angles and energies. The integration over energy extended down to 25 MeV for ^{16}O and 6 MeV for ^{4}He, at which energies the cross sections were negligible. Angular distribution coefficients were obtained also. The integration code accepts experimental branching and mixing ratios and takes into account feeding from higher excited states.

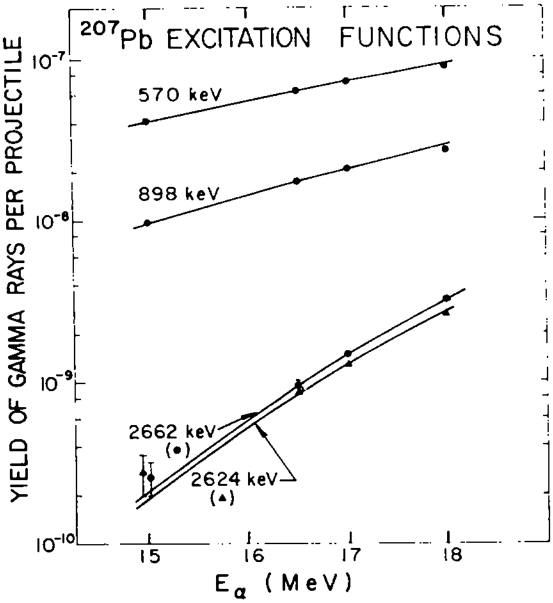

Fig. 4. Excitation functions for γ-rays originating from states at 570, 898, 2662 and 2624 keV in ^{207}Pb. The solid lines are the result of a calculation using the Winther-de Boer Coulomb excitation program. The statistical errors are smaller than the data points.

The calculated thick-target yields for E3 excitation of a state at 2.6 MeV change by about 3 % for ^{4}He and by about 16 % for ^{16}O beams assuming a change $\Delta Q_s = 1.3$ b. The ^{4}He data are thus fairly insensitive to the deformation of the states and were used (with $Q_s = 0$) to deduce accurate $B(E\lambda)$ values. Excitation functions obtained with

TABLE 1

$B(E\lambda)$ values from absolute cross sections

Nucleus	$J_i \rightarrow J_f$	E_f (keV)	Type	$B(E\lambda; J_i \rightarrow J_f)$ ($e^2 \cdot b^\lambda$)		
				this work	other work	ref.
^{204}Pb	0^+ 2^+	899.0±0.3	E2	0.151 ±0.015	0.145 ±0.015	[10]
^{206}Pb	0^+ 2^+	802.9±0.2	E2	0.095 ±0.005	0.092 ±0.006	[17]
	0^+ 3^-	2645.4±0.8	E3	0.50 ±0.03	0.66 ±0.07	[10]
					0.64 ±0.04	[12] [a]
^{207}Pb	$\frac{1}{2}^-$ $\frac{5}{2}^-$	569.6±0.1	E2	0.0214±0.0010	0.0213±0.0009	[16]
	$\frac{1}{2}^-$ $\frac{3}{2}^-$	897.7±0.3	E2	0.0121±0.0005	0.0124±0.0010	[10]
	$\frac{1}{2}^-$ $\frac{5}{2}^+$	2624.4±1.0	E3	0.23 ±0.03	0.19 ±0.02	[10]
	$\frac{1}{2}^-$ $\frac{7}{2}^+$	2662.4±0.6	E3	0.29 ±0.02	0.26 ±0.03	[10]
^{208}Pb	0^+ 3^-	2614.5±0.6	E3	0.54 ±0.03	0.72 ±0.04	[12] [a]
					0.58 ±0.04	[28]
^{209}Bi	$\frac{9}{2}^-$ $\frac{7}{2}^-$	896.5±0.3	E2	0.0024±0.0002	0.0018±0.0006	[9]
					0.0014±0.0002	[8]

[a]) From inelastic electron scattering.

^{4}He beams and a ^{207}Pb target are shown in fig. 4. The yields at 18 MeV for the 570 and 898 keV states are significantly lower than the best fit. This is somewhat surprising since the small adiabaticity parameter ξ for these states implies a much smaller increase in yield with bombarding energy than for the octupole vibrational states, which do not exhibit a sizeable deviation. In any case the 18 MeV data were not included in the analysis, as was already indicated on the basis of the γ-ray spectra. The $B(E\lambda)$ values are shown in table 1 together with the most accurate previous measurements. Corrections for internal conversion [33]) have been applied. The quoted uncertainties include $\pm 4\,\%$ for the absolute detection efficiency and $\pm 2.5\,\%$ for the stopping powers in addition to the statistical uncertainty. The agreement of our values with previous measurements is generally good except for the (ee') data in ^{206,208}Pb and the $B(E2)$ in ^{209}Bi. In the latter case our value was corrected for feeding from higher excited states (a 13 % correction at 17 MeV) yet it is nearly a factor of two larger than the one obtained by Broglia *et al.* [8]) at the rather high energy of 19 MeV.

The data for ^{204}Pb were obtained with a natural lead target and the $B(E2)$ calculated with the assumption that it contained 1.48 % of ^{204}Pb and 22.6 % of ^{207}Pb. It is of interest to note that the main E2 strength located [21]) near 4.07 MeV in ^{208}Pb, is apparently increasingly pushed down into the lower states as the mass number decreases. This trend is also indicated by the monotonic increase in the energy of the lowest 2^+ states toward lighter isotopes [34]) and by the decrease [12]) of $B(E2;\,0^+ \rightarrow 2^+$, 4.07 MeV) from ^{208}Pb to ^{206}Pb.

The accuracy of γ-ray yield measurements at the lower ^{16}O energies was limited by relatively large background, particularly for the strongly Doppler-broadened 1726 keV, $\frac{5}{2}^+ \rightarrow \frac{3}{2}^+$ transition in ^{207}Pb and the 1843 keV, $3^- \rightarrow 2^+$ transition in ^{206}Pb. The most accurate ratios of yields were obtained with ^{16}O and ^{4}He beams for the relatively sharp ($\tau \approx 1$ ps) 2093 keV, $\frac{7}{2}^+ \rightarrow \frac{5}{2}^-$ line in ^{207}Pb, yielding a static quadrupole moment $Q_s = -0.3 \pm 0.7$ b, a value smaller than that obtained by Barnett and Phillips [28]) for the 3^- state in ^{208}Pb, $Q_s = -1.3 \pm 0.6$ b. The present experiment is clearly too inaccurate to be theoretically significant. It should however be pointed out that absolute yield measurements (combined with accurate relative dE/dx measurements) can now be made with considerably improved accuracy. The 2614.5 keV, $3^- \rightarrow 0^+$ transition in ^{208}Pb is most suitable because of the long lifetime of the 3^- state ($\tau \approx 25$ ps) which eliminates significant Doppler broadening. Experiments with heavier ions such as ^{32}S or ^{35}Cl would increase the size of the reorientation effect by roughly a factor of two.

The E2/M1 mixing ratio for the 898 keV, $\frac{3}{2}^- \rightarrow \frac{1}{2}^-$ transition in ^{207}Pb was determined from angular-distribution measurements. From a fit $\delta(\frac{3}{2}^- \rightarrow \frac{1}{2}^-) = -0.075 \pm 0.025$ was obtained using the sign convention of Rose and Brink [35]). This value is in agreement with the result of the Heidelberg group [36]) yielding $\delta = (-)0.096 \pm 0.011$. A second solution for δ which corresponds to almost pure E2 is incompatible with substantial Doppler broadening of the 898 keV line. A more accurate estimate of the $\frac{3}{2}^- \rightarrow \frac{1}{2}^-$ M1 matrix element with the DSAM is described in the next section.

2.4. LIFETIMES FROM γ-RAY LINESHAPES

The velocities of Pb and Bi recoils after Coulomb excitation with ^{16}O ions extend up to $v/c \approx 0.015$. The 898, 1726 and 2093 keV lines in ^{207}Pb and the 1842 keV line in ^{206}Pb show substantial Doppler broadening, allowing the deduction of mean lifetimes for four levels by the Doppler-shift attenuation method. Theoretical line shapes were calculated on the Chalk River CDC 6600 computer for a large number of lifetimes and the best fit to the data was found from a χ^2 analysis. The methods used to calculate the lineshapes have been described before [24, 25, 37]) and only the essential features are reiterated here:

(a) For a given beam energy the correlation between the direction of the excited recoil nucleus and the direction of the γ-ray is determined by the excitation cross section and up to 15 additional angular-distribution tensors $\alpha_{k\kappa}$ ($k = 2, 4, 6$; $\kappa = 0$ to k). This information was computed using the Winther-de Boer Coulomb excitation program [32]) and stored on magnetic tape. The tensors with $k \neq 0$ are essential if line shapes at $\theta_\gamma \neq 0°$ are to be calculated. As pointed out previously [25, 37]) the line shapes observed near $\theta_\gamma = 90°$ are insensitive to the static deformation of the excited state. In all cases the counting statistics were insufficient to determine Q_s reliably at $\theta_\gamma = 0°$.

(b) The energy loss of the recoils was calculated from expressions for nuclear and electronic stopping given by Lindhardt *et al.* [38]) because the reduced velocities, $137\, v/(cZ^{\frac{2}{3}})$, do not exceed 0.12 which is about the limit for the domain of pure electronic plus nuclear stopping. The effect of nuclear scattering was taken into account only approximately following a procedure due to Warburton *et al.* [39]). The effect of nuclear scattering on the line shapes is relatively small, particularly for the shorter

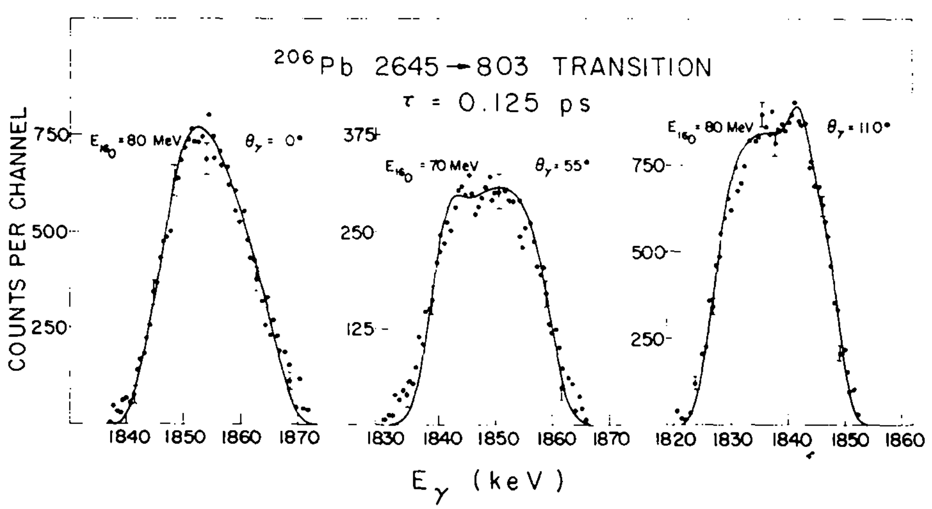

Fig. 5. Some of the γ-ray lineshapes of the $3^- \to 2^+$ E1 transition in ^{206}Pb obtained after thick-target Coulomb excitation with ^{16}O ions. The solid lines are calculated shapes assuming a mean lifetime $\tau = 0.125$ ps.

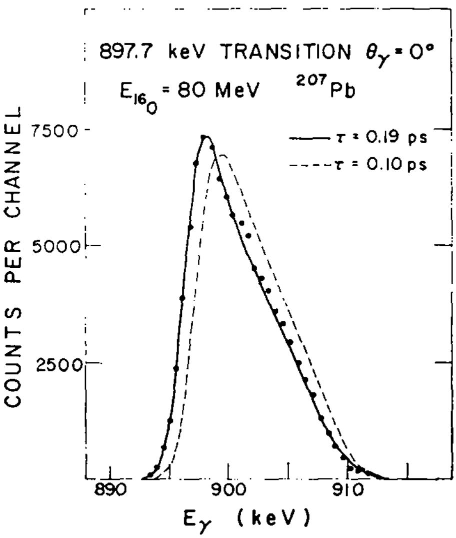

Fig. 6. Gamma-ray lineshape of the 898 keV γ-ray in ^{207}Pb observed at $\theta_\gamma = 0°$ after thick-target Coulomb excitation with 80 MeV ^{16}O. Calculated shapes for two different lifetime values are shown.

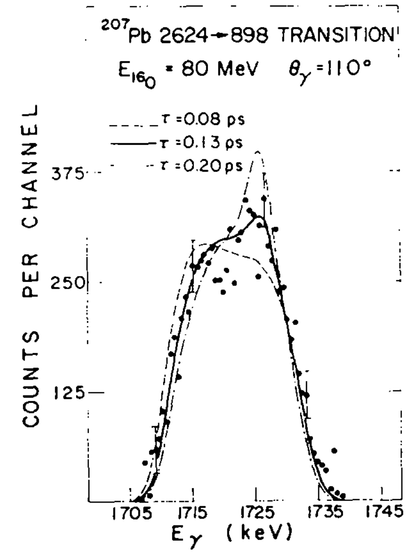

Fig. 7. Gamma-ray lineshape for the $\frac{5}{2}^+ \to \frac{3}{2}^-$ E1 transition in ^{207}Pb obtained at $\theta_\gamma = 110°$ after thick-target Coulomb excitation with 80 MeV ^{16}O ions. The solid and dashed lines are calculated shapes as discussed in the text.

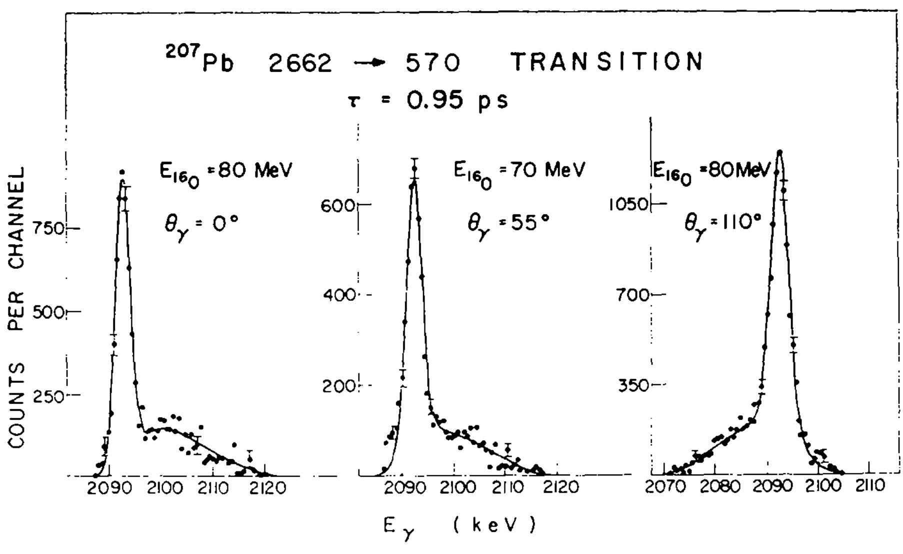

Fig. 8. Gamma-ray lineshapes of the $\frac{7}{2}^+ \to \frac{5}{2}^-$ E1 transition in ^{207}Pb observed at three angles after thick-target Coulomb excitation with ^{16}O ions. The solid lines are calculated shapes assuming a mean lifetime $\tau = 0.95$ ps.

lifetimes ($\tau \lesssim 0.2$ ps), because of the reasonably large initial recoil velocities ($v/c \lesssim 0.015$) and because recoil and target have nearly the same mass.

(c) The slowing down of the ^{16}O beam in the target was taken into account down to a cut-off energy of 25 MeV using the measured dE/dx.

(d) The resulting line shapes were folded with a Gaussian resolution function of the correct width. Spectra from monoenergetic γ-rays were used to subtract Compton distributions underlying the broadened lines [24, 25].

The shapes of the 2645 → 803, $3^- \rightarrow 2^+$ γ-ray in ^{206}Pb observed at 0°, 55° and 110° are shown in fig. 5. The 80 MeV data have also been used in the analysis, although a large fraction of the line intensity results from rather high energies between 70 and 80 MeV (about $\frac{3}{4}$ and $\frac{1}{2}$ for typical E3 and E2 excitations, respectively). As seen from fig. 5 a mean lifetime $\tau = 0.125$ ps fits both the 70 and 80 MeV data reasonably well. Our lifetime value is about a factor three smaller than the one obtained by the Heidelberg group [10]. The reason for the discrepancy is not known although it might possibly result from their neglect of the angular distribution tensors α_{kK}.

The 897.7 → 0, $\frac{3}{2}^- \rightarrow \frac{1}{2}^-$ transition in ^{207}Pb observed at $\theta_\gamma = 0°$ is shown in fig. 6. The best fit corresponding to $\tau = 0.19$ ps (solid line) differs from a distribution assuming $\tau = 0.10$ ps (dashed line) by an energy shift and a change of shape. Line shapes at 70 MeV yielded the same lifetime which is also consistent with two measurements by the Heidelberg group [10, 36] and our results for δ(E2/M1) and B(E2; $\frac{1}{2}^- \rightarrow \frac{3}{2}^-$).

For the 2624 → 898, $\frac{5}{2}^+ \rightarrow \frac{3}{2}^-$ transition in ^{207}Pb the counting statistics were poor. The lineshape obtained with 80 MeV ^{16}O at $\theta_\gamma = 110°$ was fitted with a lifetime $\tau = 0.13$ ps (see fig. 7) in qualitative agreement with ref. [10]. A considerably longer lifetime is indicated for the 2662 keV $\frac{7}{2}^+$ member of the ($\frac{1}{2}^- \otimes 3^-$) doublet in ^{207}Pb.

TABLE 2
Mean lifetimes from Coulomb excitation

Nucleus	E_{exc} (keV)	J_i	Method	τ (ps) this work	τ (ps) other expts.	ref.
^{204}Pb	899.0	2^+	TTY [b]	4.6 ±0.5	4.8 ±0.5	[10]
^{206}Pb	802.9	2^+	TTY	12.8 ±0.7	13.2 ±0.8	[17]
	2645.4	3^-	DSAM	0.125±0.030	0.4 ±0.2	[10]
^{207}Pb	569.6	$\frac{5}{2}^-$	TTY	185 ±9	186 ±5	[16]
	897.7	$\frac{3}{2}^-$	DSAM	0.19 ±0.04	0.17 ±0.05	[10]
	2624.4	$\frac{5}{2}^+$	DSAM	0.13 ±0.05	0.25 ±0.20	[10]
	2662.4	$\frac{7}{2}^+$	DSAM	0.95 ±0.20	>0.6	[10]
^{208}Pb	2614.5	3^-	TTY	27.4 ±1.5	25.5 ±1.8	[28]
^{209}Bi	896.5	$\frac{7}{2}^-$	TTY δ^2 [a]	13.3 ±2.0		

[a]) $|\delta_i|^2 = 0.37$ assumed; from ref. [19].
[b]) TTY: B(Eλ) and lifetime was deduced from thick-target yield.

Acceptable fits are obtained at $\theta_\gamma = 0°$, 55° and 110° (see fig. 8) for the 2662 → 570 γ-ray.

A summary of mean lifetimes from the present Coulomb excitation work is given in table 2. The uncertainties in the DSAM values include a 15 % uncertainty in the stopping power for the Pb recoils. The lifetimes from $B(E\lambda)$ values were corrected for internal conversion.

3. Lifetimes in ^{209}Pb and ^{209}Bi from ^{7}Li-induced reactions

The nucleus ^{209}Pb cannot be studied by Coulomb excitation and until recently no lifetimes $\lesssim$ 100 ps were known in this nucleus. The low-lying states have been studied by nucleon-transfer reactions yet these reactions produce only small recoil velocities which make them unsuitable for studies with the DSAM or the recoil-distance method. The (heavy ion, xn) reactions cannot be used since with the available targets only neutron-deficient isotopes can be strongly populated. We have made use of the comparatively large recoil velocities from the (^{7}Li, ^{6}Liγ) and the (^{7}Li, α2nγ) reactions to measure some lifetimes in ^{209}Pb and also ^{209}Bi, which had been extensively studied by Coulomb excitation [8, 9]. A detailed account of these reactions and their usefulness for lifetime measurements in other nuclei of the Pb-region may be found elsewhere [40].

A 10 mg/cm^2 thick target of ^{208}Pb was bombarded with a 60 nA, 31.5 MeV $^7Li^{3+}$ beam. A 300 μm thick annular detector was placed near 180° to detect back-scattered particles. Gamma-rays were detected in a 45 cm^3 Ge(Li) counter at θ_γ = 40°, 60°, 90°

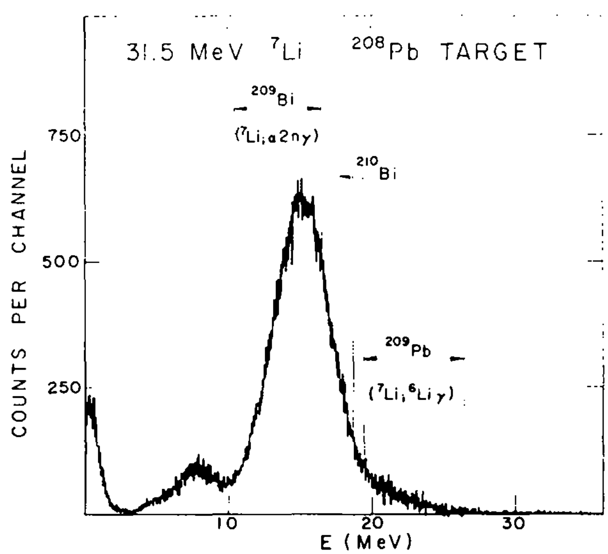

Fig. 9. Particle spectrum obtained with a 10 mg/cm^2 ^{208}Pb target and a 31.5 MeV ^{7}Li beam in coincidence with γ-rays. Random coincidences have been subtracted thus eliminating a broad peak from inelastic scattering near 25 MeV. The position of energy windows used for optimum separation of final nuclei are shown.

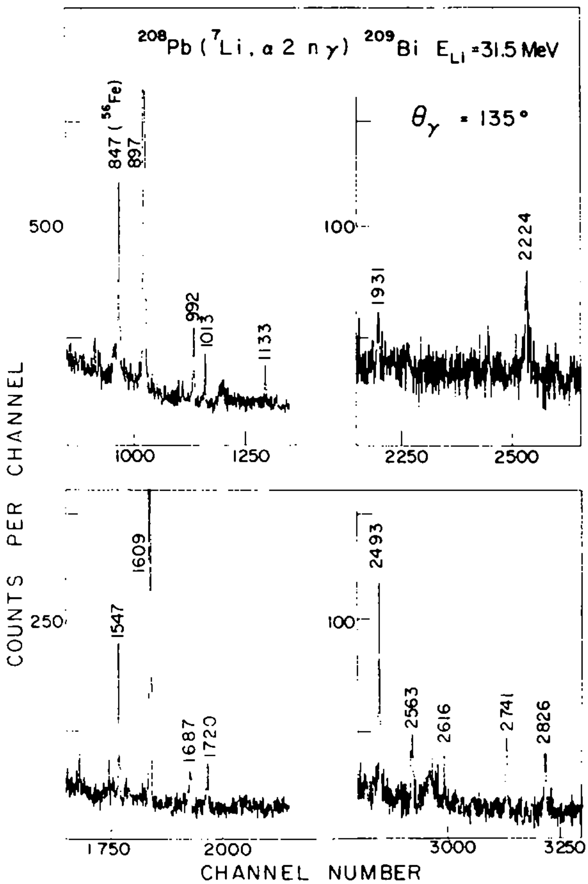

Fig. 10. Gamma-ray spectrum obtained in coincidence with the lowest energy window of fig. 9. All γ-rays indicated result from ^{209}Bi with the exception of the 847 keV and the 1013 keV lines.

and 135°. Pulse heights and time relationships were recorded on magnetic tape when γ-rays were coincident with particles. An intense, structureless, about 5 MeV wide peak, which was caused predominantly by ^{4}He, was observed near 16 MeV in the particle detector. The reason for the large cross section lies probably in the α-t cluster structure of ^{7}Li(g.s.) as discussed previously [41]). A coincidence particle spectrum, corrected for random events, is shown in fig. 9. Almost complete separation of γ-rays from ^{209}Bi, ^{210}Bi and ^{209}Pb was obtained by sorting with suitable energy windows. Particles in the low-energy ^{4}He window between $E = 10.5$ and 16.5 MeV are found to coincide with many known γ-rays in ^{209}Bi. This observation suggests a reaction of the type ^{208}Pb(^{7}Li, α2nγ)^{209}Bi which can be viewed as a (t, 2nγ) reaction with additional recoil imparted to the compound nucleus by the back-scattered ^{4}He. Gamma-rays coincident with the ^{209}Bi-particle window are shown in fig. 10. The energies of unshifted γ-ray peaks most of which can be associated with ^{209}Bi are indicated. Exceptions are lines at 847 keV, probably from ^{56}Fe(n, n'γ), and at 1013 keV, possibly from ^{27}Al(n, n'γ). The 2224 keV γ-ray results from a previously unobserved 3120 → 896.6 transition, where the initial state is most likely the $3p_{\frac{3}{2}}$ single-particle level observed near 3116 keV in the (^{3}He, d) and the (α, t) reactions [19]. The relatively strong 1547 keV line has been ascribed to a level at 3156 keV. A 1544 keV γ-ray has been observed in the (n, n'γ) reaction [42], however we have no evidence for a reported [42] 35 % branch from the 3.15 MeV level to the ground state.

From the yields and energy centroids of γ-ray lines at four angles, branching ratios and mean lifetimes were determined. The effective recoil velocity for the (^{7}Li, α2n) reaction was estimated in two ways. The (^{7}Li, α2n) reaction was simulated by a fictitious ^{208}Pb(^{7}Li, α)^{211}Bi reaction whose Q-value was varied until the α-energy coincided with the centroid of the observed α-energies calculated within the energy windows displayed in fig. 9. This assumption yielded $v/c \approx 0.0050$. Alternatively, the 2563 and 2826 keV γ-rays were known [8, 43] to be almost fully shifted, yielding $v/c = 0.00525$. The latter value was adopted for the analysis whereas the average v/c for the (^{7}Li, ^{6}Li) reaction was calculated from the known Q-values to be 0.0058. The measured F-factors were related to nuclear lifetimes by the computer code of Broude [44]) which uses the slowing-down theory of Lindhardt *et al.* [38]) and the treatment of nuclear scattering due to Blaugrund [45]). The results are summarized in table 3. The lifetimes are in good agreement with those from Coulomb excitation [8, 9]) and resonance fluorescence [43]) measurements with the possible exception of the 2601 →

TABLE 3

Lifetimes and branching ratios in ^{209}Bi and ^{209}Pb

Nucleus	E_x (keV)	$J_i \to J_f$	E_γ (keV)	Branching ratio (%)	F-factor	Mean lifetime τ(ps) this work	Mean lifetime τ(ps) other expts.	ref.
^{209}Bi	2493	$\frac{3}{2}^+ \to \frac{9}{2}^-$	2493	> 95	< 0.05	> 3	55 ± 16	[9]
	2563	$\frac{9}{2}^+ \to \frac{9}{2}^-$	2563	> 95	0.91 ± 0.04	0.020 ± 0.015	0.022 ± 0.004	[43]
	2584	$\frac{7}{2}^+ \to \frac{9}{2}^-$	2584	32	0.26 ± 0.06 (both branches)	0.44 ± 0.14	0.40 $^{+0.25}_{-0.15}$	[9]
		$\to \frac{7}{2}^-$	1687	68				
	2601	$\frac{13}{2}^+ \to \frac{13}{2}^+$	992	99 [a]	0.19 ± 0.05	0.64 ± 0.20	0.35 $^{+0.20}_{-0.15}$	[9]
	2617	$\frac{5}{2}^+ \to \frac{9}{2}^-$	2617	40	< 0.08	> 3	15 ± 5	[9]
		$\to \frac{7}{2}^-$	1720	60	< 0.05			
	2741	$\frac{15}{2}^+ \to \frac{9}{2}^-$	2741	56	< 0.05	> 3	17 ± 5	[9]
		$\to \frac{13}{2}^+$	1133	44	< 0.05			
	2826	$\frac{5}{2}^- \to \frac{9}{2}^-$	2826	60	0.99 ± 0.04	< 0.02	0.006 ± 0.002	[8]
		$\to \frac{7}{2}^-$	1930	40	1.04 ± 0.06			
	3120	$\frac{3}{2}^- \to \frac{7}{2}^-$	2224	> 95	0.88 ± 0.07	0.03 ± 0.02		
	3156	$\to \frac{13}{2}^+$	1547	> 80	< 0.05	> 3		
^{209}Pb	779	$\frac{11}{2}^+ \to \frac{9}{2}^+$	779	100	< 0.05	> 3		
	1567	$\frac{5}{2}^+ \to \frac{9}{2}^+$	1567	> 99	0.29 ± 0.04	0.47 ± 0.13		

[a]) As measured by Hertel *et al.* [9]); the shorter-lived $\frac{11}{2}^+$ member of the 2.6 MeV doublet was only populated weakly and decays mainly ($\gtrsim$ 85 %) to the ground state.

1609, $\frac{13}{2}^+ \rightarrow \frac{13}{2}^+$ transition. New lifetime estimates were obtained for the $3d_{\frac{3}{2}}$ and $3p_{\frac{1}{2}}$ single-particle states in ^{209}Pb and ^{209}Bi, respectively. The branching ratios are in good agreement with those of ref. [9]).

4. Electric transitions in ^{207,208}Pb and ^{209}Bi

The admixtures of collective components into states with predominantly simple shell-model configurations are responsible for enhanced E2 transitions observed in nuclei near closed shells. Phenomenological models for coupling the shell-model wave functions to vibrational modes of excitation have been developed by Bohr and Mottelson [46]), Choudhry [47]), de Shalit [48]) and others. The particle-vibration coupling has been particularly successful when applied [2, 8, 10, 49]) to nuclei in the lead region. We have used the intermediate-coupling unified model [47, 50]) to calculate E1 and E2 matrix elements in the three nuclei ^{207,209}Pb and ^{209}Bi. Impressive agreement with all known E2 matrix elements can be obtained with a single value of the intermediate-coupling strength. The model is however not adequate for describing E1 transitions and only qualitative agreement with observed B(E1) values was obtained. These calculations are described in the remainder of this section.

4.1 INTERMEDIATE COUPLING MODEL, B(E2) VALUES AND MIXING RATIOS

The energy eigenvalues were found from the Hamiltonian [50])

$$H = H_{\text{SM}} + H_s + H_{\text{int}},$$

where H_{SM} is the shell-model Hamiltonian for the odd nucleon moving in the effective average nuclear potential, H_s is associated with the surface energy of the surface vibration, and H_{int} is the Hamiltonian for the particle-surface interaction. Following Rustgi *et al.* [50]) we have in second quantization

$$H_s = \tfrac{1}{2}\hbar\omega \sum_{\mu} (b_\mu b_\mu^+ + b_\mu^+ b_\mu),$$

$$H_{\text{int}} = -\sqrt{\tfrac{1}{5}\pi}\,\xi\hbar\omega \sum_{\mu} (b_\mu + (-)^\mu b_{-\mu}^+) Y_{R_0\mu}(\theta, \phi),$$

where b_μ and b_μ^+ are annihilation and creation operators, respectively, for phonons of spin R and Z-component μ; ω is the frequency of the surface vibration related to the mass parameter B and the deformation parameter C by $\omega = (C/B)^{\frac{1}{2}}$; ξ is the dimensionless coupling strength related to the coupling constant k by $\xi = k(\frac{5}{2}\pi\hbar\omega C)^{\frac{1}{2}}$. The Hamiltonian H was diagonalized using eigenfunctions $|\alpha j; NR; IM\rangle$ of $H_0 = H_{\text{SM}} + H_s$ as basic vectors, i.e.

$$H_0|\alpha j;\, NR;\, IM\rangle = (E_j + N\hbar\omega)|\alpha j;\, NR;\, IM\rangle.$$

In this expression j and α are spin and other quantum numbers of the extra nucleon, N is the number of surface phonons, and $\boldsymbol{I} = \boldsymbol{R}+\boldsymbol{j}$ is the total angular momentum with Z-component M. For the off-diagonal matrix elements of H_{int} we obtain

$$\langle \alpha j';\, N'R',\, IM|H_{\text{int}}|\alpha j;\, NR;\, IM\rangle$$
$$= -\tfrac{1}{2}\xi\hbar\omega(-)^{j+j'-1}(j'\tfrac{1}{2}R_0 0|j\tfrac{1}{2})W(jR_0IR';\, j'R)\sqrt{2j'+1}\langle N'R'||b^+||NR\rangle,$$

thus defining the reduced matrix elements and coupling scheme we used. The eigenvectors $|E;\, IM\rangle$ are expanded in terms of the basis vectors, i.e.

$$|E;\, IM\rangle = \sum_{jNR} a_{jNRI}(\xi)|\alpha j;\, NR;\, IM\rangle,$$

where the expansion coefficients $a_{jNRI}(\xi)$ are found by diagonalizing H for a series of intermediate-coupling parameters ξ.

For the calculation of E2 matrix elements we have considered the core states in ^{208}Pb to be the ground state and quadrupole phonon state at 4.07 MeV, for which (e, e′) experiments have given $B(\text{E2};\, 0^+ \rightarrow 2^+) = 0.30 \pm 0.02\ e^2 \cdot \text{b}^2$.

The choice of sign for the collective matrix element is of importance if we are to calculate E2 transitions in the odd-proton nuclei ^{207}Tl and ^{209}Bi because in these nuclei the E2 matrix elements resulting from collective and from single-proton transitions can either add or subtract. This question was first discussed in detail by Rose and Brink [35]) and their formalism has been applied successfully to a number of transitions in nuclei near the ^{16}O closed shell [51–53]). We have adopted in the present work a positive sign for $\langle 12^+||b^+||00^+\rangle$, which ensures that the effective charges for

TABLE 4

E2 transitions and mixing ratios near ^{208}Pb and ^{16}O

Nucleus	$(nl_j)_i$	$(nl_j)_f$	$B(\text{E2})_{\text{exp}}$ ($e^2 \cdot \text{fm}^4$)	Intermediate coupling $\xi = 2.4$	β_{eff}	δ_{exp}	δ_{SM} [i])
^{207}Pb	$2f_{5/2}$	$3p_{1/2}$	71 ±3	71	0.94±0.02		
	$3p_{3/2}$	$3p_{1/2}$	61 ±3	65	0.80±0.02	−0.096±0.011 [f])	−0.070 β_n
	$2f_{7/2}$	$2f_{5/2}$		16		−0.085±0.013 [g])	−0.045 β_n
^{209}Pb	$3d_{5/2}$	$2g_{9/2}$	185 ±50	214	0.89±0.10		
	$4s_{1/2}$	$3d_{5/2}$	154 ±8 [a])	142	0.65±0.02		
^{209}Bi	$2f_{7/2}$	$1h_{9/2}$	30 ±3	31	2.36±0.12		
	$2f_{5/2}$	$1h_{9/2}$	480 ±170 [b])	645	0.89±0.17		
	$2f_{5/2}$	$2f_{7/2}$		0.06			positive
	$3p_{3/2}$	$2f_{7/2}$	500 $^{+1000}_{-200}$	764	$1.55^{+1.12}_{-0.35}$		
^{15}O	$1p_{3/2}$	$1p_{1/2}$				−0.17 ±0.01 [h])	−0.095 β_n
^{15}N	$1p_{3/2}$	$1p_{1/2}$	7.4±2.8 [c])		1.37±0.25 [e])	0.13 ±0.02 [h])	0.081 β_p
^{17}O	$2s_{1/2}$	$1d_{5/2}$	6.3±0.1 [d])		0.34 [e])		
^{17}F	$2s_{1/2}$	$1d_{5/2}$	64.0±1.6 [d])		1.22 [e])		

a) Ref. [15]). b) Ref. [8]). c) Ref. [57]). d) Ref. [58]).
e) $\langle 1p|r^2|1p\rangle = 7.06$ fm^2 and $\langle 2s|r^2|1d\rangle = -15$ fm^2 assumed.
f) Ref. [36]). g) Ref. [54]). h) Ref. [51]).
i) Bare-nucleon g-factors assumed.

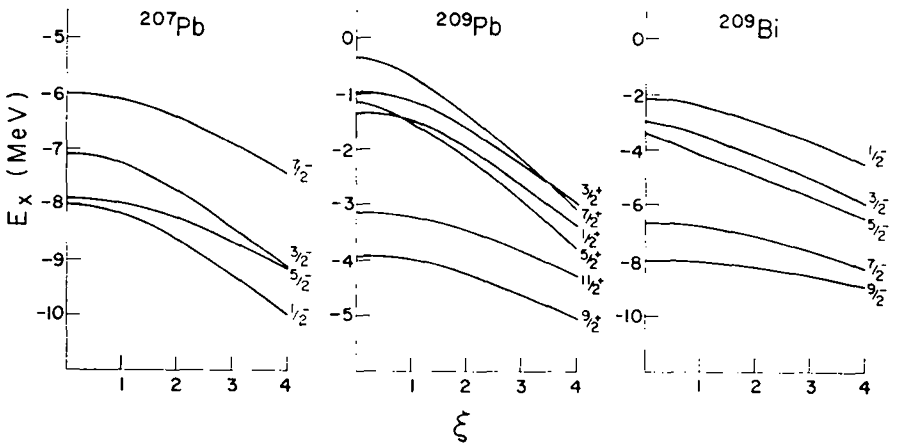

Fig. 11. Energy eigenvalues in ^{207,209}Pb and ^{209}Bi as a function of the intermediate-coupling parameter ξ. The experimentally observed level spacings are approximately reproduced near $\xi \approx 2.5$.

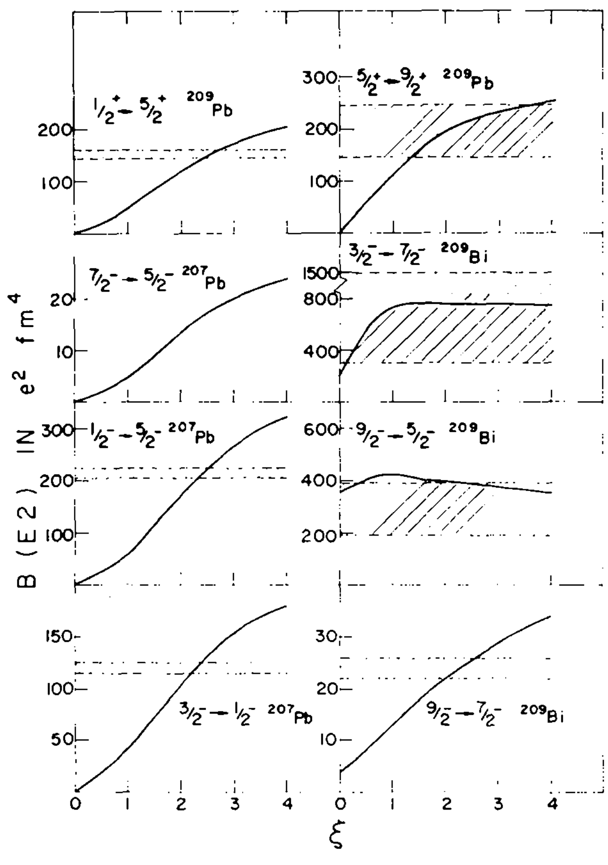

Fig. 12. B(E2) values for eight transitions between single-particle states in ^{207,209}Pb and ^{209}Bi. The solid lines are the result of an intermediate-coupling calculation; the shaded areas indicate experimental values. Except for the $B(E2; \frac{1}{2}^+ \rightarrow \frac{5}{2}^+)$ in ^{209}Pb and the $B(E2; \frac{9}{2}^- \rightarrow \frac{5}{2}^-)$ in ^{209}Bi the experimental values are from the present work (see tables 1 and 4).

E2 hole transitions in ^{207}Pb are positive, as is found in mass-15 nuclei [51]), and which reproduces the negative signs of $\delta(\frac{3}{2}^- \rightarrow \frac{1}{2}^-)$ and $\delta(\frac{7}{2}^- \rightarrow \frac{5}{2}^-)$. The sign of the latter mixing ratio was obtained by re-analyzing the original angular-distribution data of Lazar and Klema [54]) with the sign conventions of ref. [35]). All the E2/M1 mixing ratios known in ^{207}Pb and in mass-15 nuclei are contained in table 4. As expected the $\frac{3}{2}^- \rightarrow \frac{1}{2}^-$ neutron-hole transitions in ^{207}Pb and in ^{15}O have the same sign. It would be of interest to measure E2/M1 mixing ratios for transitions between single-particle (hole) states in ^{209}Bi and ^{207}Tl to see whether single-particle and collective E2 contributions are additive as is the case in ^{15}N [refs. [51–53])].

Results of the intermediate-coupling calculations are summarized in figs. 11 and 12 and table 4. The unperturbed single-particle energies have been chosen such as to reproduce approximately the experimental level scheme at an intermediate coupling strength $\xi \approx 2.5$. The B(E2) values are compared in fig. 12 and table 4. Generally good agreement is obtained for $\xi \approx 2.4$. The only possible exception is the $\frac{5}{2}^- \rightarrow \frac{9}{2}^-$ E2 transition in ^{209}Bi measured by Broglia *et al.* [8]). It should, however, be noted that their value for $B(\mathrm{E2}; \frac{9}{2}^- \rightarrow \frac{7}{2}^-)$ is almost a factor of two lower than determined by the present experiment (see table 1). Also shown in table 4 is the effective charge for E2 transitions, evaluated using harmonic oscillator eigenfunctions with an oscillator parameter $b^2 = m\omega/\hbar = 5.324$ fm^2. Since all states considered here are bound by

TABLE 5

Intermediate-coupling wave functions for ^{207,209}Pb and ^{209}Bi at $\xi = 2.4$

^{207}Pb	E (keV)	$(nl_j)_{\mathrm{SM}}$	SM	$p_{\frac{1}{2}} \otimes 2^+$	$p_{\frac{3}{2}} \otimes 2^+$	$f_{\frac{5}{2}} \otimes 2^+$	$f_{\frac{7}{2}} \otimes 2^+$		
	0	$3p_{\frac{1}{2}}$	0.926		0.218	0.309			
	570	$2f_{\frac{5}{2}}$	0.948	0.206	−0.092	−0.215	0.062		
	898	$3p_{\frac{3}{2}}$	0.919	−0.219	−0.180	0.140	0.236		
	2340	$2f_{\frac{7}{2}}$	0.927		0.285	0.122	0.210		
^{209}Pb				$s_{\frac{1}{2}} \otimes 2^+$	$d_{\frac{3}{2}} \otimes 2^+$	$d_{\frac{5}{2}} \otimes 2^+$	$g_{\frac{7}{2}} \otimes 2^+$	$g_{\frac{9}{2}} \otimes 2^+$	$i_{\frac{11}{2}} \otimes 2^+$
	0	$2g_{\frac{9}{2}}$	0.960			0.153	−0.034	−0.228	0.047
	778	$1i_{\frac{11}{2}}$	0.959				0.157	−0.060	−0.228
	1566	$3d_{\frac{5}{2}}$	0.840	0.158	−0.078	−0.162	0.058	0.484	
	2032	$4s_{\frac{1}{2}}$	0.923		0.237	0.302			
	2493	$2g_{\frac{7}{2}}$	0.834		0.191	−0.066	−0.163	0.145	0.465
	2539	$3d_{\frac{3}{2}}$	0.921	−0.196	−0.180	0.123	0.258		
^{209}Bi				$p_{\frac{1}{2}} \otimes 2^+$	$p_{\frac{3}{2}} \otimes 2^+$	$f_{\frac{5}{2}} \otimes 2^+$	$f_{\frac{7}{2}} \otimes 2^+$	$h_{\frac{9}{2}} \otimes 2^+$	$h_{\frac{11}{2}} \otimes 2^+$
	0	$1h_{\frac{9}{2}}$	0.963			0.126	−0.048	−0.230	0.025
	897	$2f_{\frac{7}{2}}$	0.951		0.125	−0.045	−0.214	0.089	0.158
	2826	$2f_{\frac{5}{2}}$	0.704	0.093	−0.056	−0.123	0.105	0.683	
	3120	$3p_{\frac{3}{2}}$	0.771	−0.116	−0.132	0.097	0.605		
	3640, 4421	$3p_{\frac{1}{2}}$	0.880		0.274	0.388			

several MeV, the radial integrals agree well with those from a more realistic Woods-Saxon potential [55]. It is seen that the effective charges are not constant and therefore the intermediate-coupling model is more appropriate. The reason for the success of the intermediate-coupling model lies probably in the localization of the main E2 strength in the 4.07 MeV ^{208}Pb state which is sufficiently collective that the neglect of antisymmetrization in the model is not very serious.

The encouraging agreement for the E2 transitions allows a reasonable estimate of the amount of collective admixtures in the single-particle (hole) states in ^{207,209}Pb and ^{209}Bi to be made. The wave functions for a number of levels are shown in table 5. The collective components amount to typically 15 % as compared with an estimated ≈ 10 % for the single-hole states in mass-15 nuclei [56]. The present calculation overestimates the collective admixtures since we neglect unidentified E2 strength above 4 MeV in ^{208}Pb. On the other hand we have not considered possible other particle-core coupling configurations, and excitations of $i_{13/2} \to i_{11/2}$ (neutron) and $h_{11/2} \to h_{9/2}$ (proton) which are important for calculations of M1 transition rates.

4.2. ELECTRIC DIPOLE AND OCTUPOLE TRANSITIONS

The low-lying collective states in ^{209}Bi and ^{207}Pb that arise from weak coupling of the lowest single-particle (hole) configuration to the octupole vibrational state at 2.6 MeV in ^{208}Pb, decay by E1 or E3 transitions to lower-lying shell-model states. The E1 and E3 strengths are summarized in tables 6 and 7, respectively. The B(E1) values are seen to be more than four orders of magnitude weaker than the giant dipole strength located [59] near 13 MeV in ^{208}Pb with $B(\mathrm{E1}; 1^- \to 0^+) \approx 20\ e^2 \cdot \mathrm{fm}^2$.

TABLE 6

E1 transitions in ^{207}Pb and ^{209}Bi

Nucleus	$J_i \to J_f$	$B(\mathrm{E1}; J_i \to J_f)$ [a] ($e^2 \cdot \mathrm{fm}^2$)	Present [b] model	Hamamoto [c]
^{207}Pb				
	$\frac{7}{2}^+ \to \frac{5}{2}^-$	(7.2±1.5) (−5)	25 (−5)	
	$\frac{5}{2}^+ \to \frac{5}{2}^-$	<4 (−5)	3.2 (−6)	
	$\frac{5}{2}^+ \to \frac{3}{2}^-$	(9.4±3.6) (−4)	14 (−4)	
^{209}Bi				
	$\frac{11}{2}^+ \to \frac{9}{2}^-$	(1.0±0.3) (−3)	1.6 (−7)	0.3 (−3)
	$\frac{9}{2}^+ \to \frac{9}{2}^-$	(1.7±0.3) (−3)	0.22 (−3)	0.55 (−3)
	$\frac{9}{2}^+ \to \frac{7}{2}^-$	<3 (−4)	3.7 (−5)	1.6 (−5)
	$\frac{7}{2}^+ \to \frac{9}{2}^-$	(2.6±0.9) (−5)	2.2 (−5)	0.75 (−5)
	$\frac{7}{2}^+ \to \frac{7}{2}^-$	(2.0±0.7) (−4)	2.7 (−4)	0.6 (−4)
	$\frac{5}{2}^+ \to \frac{7}{2}^-$	(4.9±1.7) (−6)	1.1 (−4)	1.1 (−6)

[a] Powers of ten in parenthesis: the ^{209}Bi values are taken from refs. [9,43]; the ^{207}Pb values are from the present work.

[b] $B(\mathrm{E2}; 2^+ \to 3^-) = 8 \cdot 10^{-3}\ e^2 \cdot \mathrm{fm}^4$ assumed; effective charge for E1 transition 0.3 and 0.065 for ^{207}Pb and ^{209}Bi, respectively.

[c] Ref. [2].

TABLE 7

E3 transitions in ^{207,208}Pb and ^{209}Bi

Nucleus	J_x^π	$E_x - 2614.5$ (keV)	$B(\text{E3}; J_x \rightarrow J_{\text{g.s.}})$ ($e^2 \cdot \text{b}^3$)	
			[a]	[b]
^{208}Pb	3^-	0	0.0771 ± 0.0043	(0.0771)
^{207}Pb	$\frac{7}{2}^+$	+48	0.0725 ± 0.0050	0.0730
	$\frac{5}{2}^+$	+10	0.0767 ± 0.0100	0.0726
^{209}Bi	$\frac{3}{2}^+$	−122	0.053 ± 0.007	
	$\frac{9}{2}^+$	−51	0.074 ± 0.011	
	$\frac{7}{2}^+$	−32	0.065 ± 0.010	
	$\frac{11}{2}^+$	−15	0.078 ± 0.012	
	$\frac{13}{2}^+$	−13	0.072 ± 0.011	
	$\frac{5}{2}^+$	+2	0.057 ± 0.009	
	$\frac{15}{2}^+$	+127	0.048 ± 0.007	

[a]) The data on ^{207,208}Pb are from the present work; the data on ^{209}Bi are from Hertel *et al.* [9]).
[b]) Hamamoto, ref. [2]).

Therefore E1 transitions are expected to be very sensitive to small admixtures in their wave functions. The most important admixtures contributing to E1 transitions between collective $|j_c\rangle$ and shell-model $|j_s\rangle$ states are probably

$$|j_c\rangle = a_0|(\alpha j) \otimes 3^-\rangle + a_1|(\alpha' j) \otimes 0^+\rangle + a_2|(\beta j_s) \otimes 1^-\rangle + \ldots,$$

$$|j_s\rangle = b_0|(\beta j_s) \otimes 0^+\rangle + b_1|(\alpha j) \otimes 2^+\rangle + \ldots,$$

where a_0, $b_0 > 0.7$. Previous calculations of E1 matrix elements by Hamamoto [2]) have only considered single-particle (hole) admixtures $|(\alpha' j)\rangle$ into the collective state. Then the reduced matrix element for E1 transitions is $a_1 b_0 \langle \alpha' j || (\text{E1}) || \beta j_s \rangle$. Typically $|a_1|^2 = 0.01$, and this implies that the E1 transition rate is reduced by a large amount. Alternatively, Broglia *et al.* [8]) have shown that several E1 transition strengths in ^{209}Bi can be fitted by including the $|(\alpha j) \otimes 2^+\rangle$ admixtures and by adjusting individually the coupling strength to the 1^- giant dipole state.

We have calculated the E1 transition strengths using the intermediate-coupling wave functions $|j_s\rangle$ from table 5. The small single-particle (hole) admixtures $|(\alpha' j_c)\rangle$ in the collective states were taken from the work of Hamamoto [2]). Configurations of the type $|(\beta j_s) \otimes 1^-\rangle$ were neglected to avoid the introduction of more parameters in H_{int} and to circumvent problems of antisymmetrization arising from the predominant particle-hole structure of both the 3^- and 1^- states. The values of table 6 were obtained assuming $B(\text{E2}; 2^+ \rightarrow 3^-) = 0.008\ e^2 \cdot \text{fm}^2$ and different effective E1 charges in ^{207}Pb and ^{209}Bi. The agreement for some ^{209}Bi transitions is poor, however a modest variation of the effective E1 charge could have reduced the discrepancies considerably. The E1 transition strengths in ^{207}Pb are qualitatively reproduced, particularly the difference in the lifetimes of the $\frac{7}{2}^+$ and $\frac{5}{2}^+$ states.

The B(E3) values in ^{207,208}Pb from the present work and in ^{209}Bi from ref. [9]) are shown in table 7. The simple weak-coupling model which predicts equal $B(\mathrm{E3}, J \rightarrow \mathrm{g.s.})$ is seen to work well. The largest reduction in E3 strength occurs for the $J = \frac{3}{2}^+$ and $\frac{15}{2}^+$ members of the ^{209}Bi septuplet which also exhibit the largest energy shift.

5. Magnetic dipole transitions

The information from present and previous work on lifetimes, branching ratios and mixing ratios in ^{207,209}Pb and ^{209}Bi can be combined to provide eight transition probabilities for M1 decay. These B(M1) values are listed in table 8 together with theoretical predictions which will be described below. Five of the transitions are between states of predominantly single-particle (hole) character and two of those are forbidden by l-selection rules. The probabilities for the allowed transitions are compared in table 8 to those of the extreme shell model in which pure configurations and free-nucleon g-factors are assumed. The experimental B(M1) values are smaller by factors of between two and four, a most interesting observation in view of the known deviations of magnetic moments near ^{208}Pb from the Schmidt values.

It should first be remarked that the coupling of a particle (hole) to quadrupole or octupole phonons, which have been shown to describe extremely well the E2 and E3

TABLE 8

M1 transitions in ^{207,209}Pb and ^{209}Bi

Nucleus	$J_i \rightarrow J_f$	E_γ (keV)	τ(M1) (ps)	$B(\mathrm{M1})\ (\mu_n^2)$ exp	Shell [g]) model	theory
^{207}Pb	$\frac{3}{2}^- \rightarrow \frac{1}{2}^-$	897.7	0.19 ± 0.03	0.41 ± 0.07	1.16	0.30(0.26) [e])
	$\frac{7}{2}^- \rightarrow \frac{5}{2}^-$	1771	0.021 ± 0.007 [a])	0.49 ± 0.16	1.50	0.14(0.12) [e])
^{209}Pb	$\frac{11}{2}^+ \rightarrow \frac{9}{2}^+$	779	> 3	< 0.04	0	$10.0(9.2) \cdot 10^{-3}$ [e])
^{209}Bi	$\frac{5}{2}^- \rightarrow \frac{7}{2}^-$	1930	0.0106 ± 0.0020 [b])	0.76 ± 0.15	2.86	0.90(0.61) [e])
	$\frac{7}{2}^- \rightarrow \frac{9}{2}^-$	896.6	18.2 ± 3 [c])	$(4.3 \pm 0.7)10^{-3}$	0	$2.5(2.3) \cdot 10^{-2}$ [e])
	$\frac{11}{2}^+ \rightarrow \frac{13}{2}^+$	992	0.41 ± 0.12 [d])	0.14 ± 0.04		$4.9(3.7) \cdot 10^{-2}$ [f])
	$\frac{13}{2}^+ \rightarrow \frac{13}{2}^+$	993	0.64 ± 0.20	0.09 ± 0.03		0.014(0.077) [f])
	$\frac{15}{2}^+ \rightarrow \frac{13}{2}^+$	1133	38.6 ± 11.4 [h])	$(1.0 \pm 0.3)10^{-3}$		$5.8(108) \cdot 10^{-3}$ [f])

[a]) Use $B(\mathrm{E2};\ \frac{7}{2}^- \rightarrow \frac{5}{2}^-) = 16.3\ e^2 \cdot \mathrm{fm}^4$ from the intermediate-coupling calculation ($\xi = 2.4$) and $\delta = -0.085 \pm 0.013$ from ref. [54]).

[b]) Use $B(\mathrm{E2};\ \frac{5}{2}^- \rightarrow \frac{9}{2}^-) = 645\ e^2 \cdot \mathrm{fm}^4$ from the intermediate-coupling calculation ($\xi = 2.4$) and branching ratio of table 3.

[c]) Use measured $B(\mathrm{E2};\ \frac{7}{2}^- \rightarrow \frac{9}{2}^-)$ and $\delta = 0.37$ from ref. [19]).

[d]) Use $T_{\frac{1}{2}}(\frac{11}{2}^+) = 0.043 \pm 0.012$ from ref. [19]) and branching ratio of table 3.

[e]) Numbers in brackets include reduction of amplitude of single-particle states due to particle-core coupling.

[f]) Numbers in brackets obtained with $g_{3^-} = 0$.

[g]) Pure configurations and free-nucleon g-factors assumed.

[h]) Lifetime of $\frac{15}{2}^+$ state taken from ref. [9]), branching ratio taken from the present work.

matrix elements in mass-207 and mass-209 nuclei, is not well suited for calculations of M1 matrix elements. If we assume a vanishing magnetic moment of the 2^+ and 3^- phonon states, the only effect of the particle-core coupling on M1 transitions is through the reduction in the amplitudes for the single-particle shell-model states. Typically for the amplitude given in table 5 this leads to a reduction of B(M1) by only ≈ 20 %. Assuming a magnetic moment of a particular sign for the 2^+ or 3^- state can lead to further reduction of B(M1); for example in ^{207}Pb, the magnetic moments of the $\frac{1}{2}^-$ and $\frac{3}{2}^-$ states and $B(\mathrm{M1}; \frac{3}{2}^- \rightarrow \frac{1}{2}^-)$ could be brought into agreement with experiment if we assumed $g_{2^+} = -0.4$. Such a large negative g-factor for a collective state seems however highly implausible (collective states with a very large number of configurations are expected to have the "random" g-factor $+Z/A$) and would have to be justified by a detailed microscopic description of the phonon state.

A physically more meaningful explanation of the retardation of M1 matrix elements and magnetic moments is provided if one considers the polarization of the core by the valence nucleon. This polarization is brought about by the short-range nucleon-nucleon force which gives rise to $1\hbar\omega$ excitations of spin-orbit partners $(j_p j_h^{-1})$. In the region of ^{208}Pb there are two particle-hole states, $1i_{\frac{11}{2}}$-$1i_{\frac{13}{2}}$ (neutrons) and $1h_{\frac{9}{2}}$-$1h_{\frac{11}{2}}$ (protons), that can give rise to a renormalization of the M1 and μ operators. The contribution from core excitation, Δ, can be evaluated with the formalism of effective operators [60], which yields in first-order perturbation theory [for the exact expression see ref. [60]]:

$$\Delta(\mu \text{ or M1}) \approx -\langle j j_h | V_{12} | j' j_p \rangle \frac{1}{\varepsilon_p - \varepsilon_h} \langle j_p | \text{M1 or } \mu | j_h \rangle.$$

The corresponding diagram is shown in figs. 13b and c, the curly line being the antisymmetrized two-body reaction matrix element of the interaction V_{12} and the dashed line indicating the M1 or μ operator. A general qualitative argument can be given which shows that Δ has the opposite sign of the single-particle (hole) matrix elements shown in fig. 13a. Consider the case where the valence nucleon is a proton (neutron).

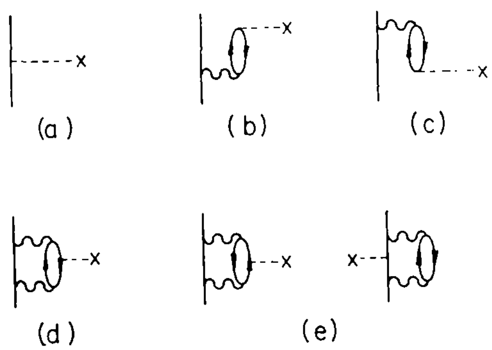

Fig. 13. Diagrams for (a) single-particle contribution; (b) and (c) first-order renormalization; (d) and (e) some of the second-order diagrams that contribute to M1 renormalization.

The reaction matrix element for excitation of a neutron (proton) particle-hole pair is negative because it is dominated by the attractive triplet-even states. On the other hand excitation of a proton (neutron) particle-hole pair implies a positive reaction matrix element since the attractive force between $^1S_0$ states cannot contribute because of angular-momentum restrictions. Furthermore, since the M1 or μ matrix element changes sign in going from neutron to proton spin-orbit partners and the spin-orbit splitting $\varepsilon_p - \varepsilon_h$ is always positive, the contributions of neutron and proton pairs to Δ are additive, reducing both the magnetic moments and the M1 transition probabilities from the single-particle configurations.

The renormalization of magnetic moments in ^{207}Pb and ^{209}Bi due to core polarization has been estimated previously [20, 21, 61]) with a variety of potentials. We have performed a similar calculation and extended it to M1 transitions using the separable non-local potential of Kahana *et al.* [62]) and the formalism of ref. [60]). A spin-orbit splitting of 4.89 MeV ($1h_{9/2}$-$1h_{11/2}$) for protons and 5.22 MeV ($1i_{11/2}$-$1i_{13/2}$) for neutrons was assumed. The B(M1) values for transitions in ^{207,209}Pb and ^{209}Bi were renormalized in this way and are shown in table 8. The corrected magnetic moments of shell-model states in ^{207}Pb and ^{209}Bi are given in table 9 together with the results of previous calculations [20, 21]).

TABLE 9

Magnetic moments in ^{207}Pb and ^{209}Bi [a])

Nucleus	State	μ_{SM}	μ_{exp}	Present work	Blomqvist *et al.* [20])	Mavromatis and Zamick [21])
^{207}Pb	$3p_{1/2}^{-1}$	0.64	0.59	0.61	0.45	0.63
	$2f_{5/2}^{-1}$	1.37	0.65±0.05 [b])	0.88	0.91	
	$3p_{3/2}^{-1}$	−1.91		−1.07		
	$2f_{7/2}^{-1}$	−1.91		−1.08		
^{209}Bi	$1h_{9/2}$	2.62	4.08	3.76	3.34	3.42

[a]) In nuclear magnetons.

[b]) Ref. [16]).

In ^{207}Pb this approach explains the deviations of the magnetic moments of the $3p_{1/2}^{-1}$ and $2f_{5/2}^{-1}$ states from the single-particle moments rather well. The small differences of our calculated values from previous work by Blomqvist *et al.* [20]) and by Mavromatis *et al.* [21]) must be attributed mainly to differences in the realistic nucleon-nucleon interaction and to our slightly smaller spin-orbit splitting. The renormalization of the magnetic moments of the $\frac{5}{2}^-$ state in ^{207}Pb and especially of the ^{209}Bi ground state turns out to be too small. On the other hand the core polarization contribution is too large in the case of M1 transition rates. A large discrepancy is observed for the allowed $2f_{7/2}^{-1} \rightarrow 2f_{5/2}^{-1}$ transition in ^{207}Pb which is retarded by about a factor of three whereas the present calculation yields a retardation by a factor of ten (table 8). A similarly large disagreement is observed for the M1 transition between the $2f_{7/2}$ and $1h_{9/2}$ states in ^{209}Bi, for which the M1 matrix element in the simple shell model (fig. 13a) is identically zero. However figs. 13b and c do contribute and yield a $B(\text{M1})$ of 0.023 nuclear megnetons, which is larger than the experimental result by about a factor five. Another l-forbidden M1 transition occurs between the $1i_{\frac{11}{2}}$ and $2g_{\frac{9}{2}}$ states in ^{209}Pb with a $B(\text{M1})$ determined by the experimental limits on the mean lifetime of the 779 keV state, 3ps < τ < 1 ns. Using the calculated $B(\text{M1})$ and a calculated $B(\text{E2}; \frac{11}{2}^+ \rightarrow \frac{9}{2}^+) = 7.9\ e^2 \cdot \text{fm}^4$ obtained with the wave functions of table 5, the expected lifetime is $\tau(779\ \text{keV}) = 11.7$ ps consistent with the experimental limits. An accurate measurement of this lifetime would appear worthwhile.

The partial success of the first-order core polarization picture raises the very interesting question for the origin of the remaining discrepancies. Second- (and higher-) order contributions from diagrams such as shown in figs. 13d and e can certainly be significant and provide a modification of the first-order result. There are a very large number of particle-hole states that can contribute in second order, and unless the signs are randomly distributed and the magnitudes are similar, these diagrams could alter the results given in tables 8 and 9 considerably. The second-order contributions have been evaluated by Mavromatis and Zamick [21]) for the magnetic moment of the ^{209}Bi ground state and amount to -0.21 nuclear magnetons thus worsening the agreement with experiment. The contribution from mesonic exchange currents between any two nucleons can be very significant and has been estimated [22]) to contribute ≈ 0.5 nuclear magnetons to $\mu(^{209}\text{Bi})$ which is nearly of the same order of magnitude as the core polarization contribution. It can therefore be hoped that a combination of exchange currents and higher-order core polarization terms will provide improved calculations of magnetic moments and M1 transition rates.

The three known M1 transitions from the $\frac{11}{2}^+$, $\frac{13}{2}^+$ and $\frac{15}{2}^+$ members of the $(3^- \otimes h_{\frac{9}{2}})$ septuplet in ^{209}Bi to the first $\frac{13}{2}^+$ state at 1.608 MeV present another interesting problem. Hamamoto has calculated the energy shift and wave function of this septuplet by mixing with the single-particle states $1i_{\frac{13}{2}}$, $1i_{\frac{11}{2}}$. We have calculated the $B(\text{M1})$ values for these states using Hamamoto's wave functions and assuming $g_{3^-} = 0.58 \pm 0.14$, $g_l = 1$ and $g_s = 0.35\ g_s^{\text{free}}$ where $g_s^{\text{free}} = 5.88$. As shown in table 8 the results are not in good agreement with the experimental values. We have also calculated these three $B(\text{M1})$ values for the case $g_{3^-} = 0$; although this gives numbers which are closer to experiment, there is still a large discrepancy. It ought to be emphasized that the particle-core-coupling models do not lead to sufficient renormalization effects for magnetic dipole strengths, or for magnetic moments, and the magnitudes of these small $B(\text{M1})$ values provide a very sensitive test of the small components in the wave functions of these states. Thus a more realistic calculation of these M1 transition probabilities will require a microscopic description of the octupole vibrational states.

6. Conclusions

The present experiments have determined a number of electromagnetic matrix elements in nuclei near ^{208}Pb. Absolute cross sections from Coulomb excitation with

^{4}He and ^{16}O beams were measured in five nuclei. The extracted B(E2) and B(E3) values are accurate to at best ± 5 % and are found in reasonable agreement with other recent measurements. Four Doppler-broadened γ-ray lineshapes observed after bombardment with the ^{16}O beam at several angles were interpreted by the DSAM. The ^{7}Li-induced transfer reactions have been shown to provide a promising way for measuring lifetimes with $\tau < 10$ ps in heavy nuclei. The ^{208}Pb(^{7}Li, $\alpha 2n\gamma$)^{209}Bi reaction has been used to extract a number of lifetimes in ^{209}Bi and good agreement with previous work using Coulomb excitation and resonance fluorescence was obtained.

The good accuracy of B(E2) and B(E3) values in ^{207}Pb, ^{209}Pb and ^{209}Bi allows a sensitive test of particle-core-coupling models in the Pb region to be made. An intermediate coupling calculation has successfully accounted for all known B(E2) values with a unique value of the coupling strength. The collective components in the wave functions of the lowest single-particle (hole) states are typically ≈ 15 % and give a fair idea of the quality of the shell closure in the ^{208}Pb ground state. It is worth mentioning that this information cannot be obtained from single-nucleon-transfer reactions to the states in question, even if spectroscopic factors could be measured with high accuracy. Spectroscopic factors of about unity are obtained whether the relevant states are good single-particle (hole) states in a closed core or a strongly correlated core. This is because, among the very large number of (Np-Nh) excitations that contribute to the correlated ground state, the occupation number for any particular particle (hole) is expected to be very small. Therefore, our relatively large estimate for collective admixtures is not in contradiction with spectroscopic factors of ≈ 1 quoted in the literature [1]).

The intermediate-coupling model is found to be quite inadequate for giving good values for B(E1) and B(M1). The B(E1) values depend quite sensitively on the small admixtures of single-particle and other particle-hole states. Reasonable estimates have been made by including single-particle components in the multiplets obtained by coupling single-particle states ($p_{\frac{1}{2}}$ for ^{207}Pb and $h_{\frac{9}{2}}$ for ^{209}Bi) to the 3^- phonon and assuming a reasonable value for $B(\text{E1}; 2^+ \rightarrow 3^-)$ in ^{208}Pb. The need for an E1 effective charge suggests that the model is still quite crude and some effects from the giant dipole states should be included. Coupling to 2^+, 3^- and 1^- phonon states seems to be a reasonable idea but is so complicated that a microscopic calculation might just as well be undertaken.

The particle-core-coupling model is completely inadequate for calculating magnetic moments and B(M1). The structure of the magnetic-moment operator indicates that it is the spin-orbit partners in a shell which give rise to its renormalization whereas the core-coupling model uses the quadrupole phonon state made up primarily of $2\hbar\omega$ excitations. The portions of the Hilbert space spanned by M1 and E2 operators are quite different. Therefore we have calculated the renormalization of the three allowed M1, two l-forbidden M1 and three magnetic moments (in ^{207}Pb and ^{209}Bi) in the first-order perturbation theory. In all eight cases this procedure explains qualitatively the observed deviations from the extreme shell-model picture although some quantitative discrepancies remain. Perhaps the source of these discrepancies can be attributed to second- and higher-order renormalization and to the effects of meson exchange currents. Certainly the last two contribute significantly to the renormalization of the ground state magnetic moment of ^{209}Bi. No doubt the renormalization of magnetic moments and M1 transition rates provides a more challenging theoretical problem.

References

1) N. Stein, in Proc. Int. Conf. on properties of nuclear states, Montreal, 1969, p. 337; see many references therein
2) I. Hamamoto, Nucl. Phys. **A126** (1969) 545; Nucl. Phys. **A141** (1970) 1; Nucl. Phys. **A148** (1970) 465
3) C. Ellegaard, J. Kantele and P. Vedelsby, Nucl. Phys. **A129** (1969) 113
4) C. Ellegaard and P. Vedelsby, Phys. Lett. **26B** (1968) 115
5) G. R. Satchler, W. C. Parkinson and D. L. Hendrie, Phys. Rev. **187** (1969) 1491
6) W. C. Parkinson, O. L. Hendrie, H. H. Duhm, J. Mahoney, J. Saudinos and G. R. Satchler, Phys. Rev. **178** (1969) 1976
7) C. A. Whitten, Jr., N. Stein, G. E. Holland and D. A. Bromley, Phys. Rev. **188** (1969) 1941
8) R. A. Broglia, J. S. Lilley, P. Perazzo and W. R. Phillips, Phys. Rev. **C1** (1970) 1508
9) J. W. Hertel, D. G. Fleming, J. P. Schiffer and H. E. Gove, Phys. Rev. Lett. **23** (1969) 488
10) E. Grosse, M. Dost, K. Haberkant, J. W. Hertel, H. V. Klapdor, H. J. Körner, D. Proetel and P. von Brentano, Nucl. Phys. **A174** (1971) 525
11) M. H. McFarlane, in Proc. Int. Conf. on properties of nuclear states, Montreal, 1969, p. 385
12) J. F. Ziegler and G. A. Peterson, Phys. Rev. **165** (1968) 1337
13) O. Nathan, Nucl. Phys. **30** (1962) 332
14) D. S. Andreev, J. Z. Gangrskij, I. C. Lemberg and V. A. Nabinoritschvili, Izv. Akad. Nauk SSSR (ser. fiz.) **29** (1965) 2231
15) P. Salling, Phys. Lett. **17** (1965) 139
16) H. J. Körner, K. Auerbach, J. Braunsfurth and E. Gerdau, Nucl. Phys. **86** (1966) 395
17) J. L. Quebert, K. Nakai, R. M. Diamond and F. S. Stephens, Nucl. Phys. **A150** (1970) 68
18) O. Häusser and D. Ward, Atomic Energy of Canada Limited reports AECL-3668 (1970) and AECL-3865 (1970)
19) M. R. Schmorak and R. L. Auble, Nucl. Data **B5** (1971) 207;
M. J. Martin, Nucl. Data **B5** (1971) 287
20) A. Arima and H. Horie, Prog. Theor. Phys. **A1** (1954) 509;
J. Blomqvist, N. Breed and H. O. Zetterström, Phys. Lett. **18** (1965) 47
21) H. A. Mavromatis, L. Zamick and G. E. Brown, Nucl. Phys. **80** (1966) 545;
H. A. Mavromatis and L. Zamick, Nucl. Phys. **A104** (1967) 17
22) M. Chemtob, Nucl. Phys. **A123** (1969) 449
23) F. C. Khanna, to be published
24) O. Häusser, D. Pelte, T. K. Alexander and H. C. Evans, Can. J. Phys. **47** (1969) 1065
25) D. Pelte, O. Häusser, T. K. Alexander and H. C. Evans, Can. J. Phys. **47** (1969) 1929
26) C. Broude, Atomic Energy of Canada Limited report AECL-3512 (1969)
27) T. Yamazaki, Phys. Rev. **C1** (1970) 290
28) A. R. Barnett and W. R. Phillips, Phys. Rev. **186** (1969) 1205
29) L. C. Northcliffe and R. F. Schilling, Nucl. Data **A7** (1970) 233
30) C. F. Williamson, J. P. Boujot and J. Picard, rapport CEA-R 3042 (1966)
31) W. Booth and I. S. Grant, Nucl. Phys. **63** (1965) 481
32) A. Winther and J. de Boer, in Coulomb excitation, ed. K. Alder and A. Winther (Academic Press, New York, 1966)
33) M. E. Rose, Internal conversion coefficients, (North-Holland, Amsterdam, 1958)
34) A. Hanser, Nucl. Phys. **A146** (1970) 241

35) H. J. Rose and D. M. Brink, Rev. Mod. Phys. **39** (1967) 306
36) H. V. Klapdor, P. von Brentano, E. Grosse and K. Haberkant, Nucl. Phys. **A152** (1970) 263
37) D. Pelte, O. Häusser, T. K. Alexander, B. W. Hooton and H. C. Evans, Phys. Lett. **29B** (1969) 660
38) I. Lindhardt, M. Scharff and H. E. Schiott, Mat. Fys. Medd. Dan. Vid. Selsk. **33** (1963) No. 14
39) E. K. Warburton, J. W. Olness and A. R. Poletti, Phys. Rev. **160** (1967) 938
40) D. Ward and O. Häusser, Atomic Energy of Canada Limited reports AECL-3865 (1970), AECL-3996 (1971);
A. Olin, D. Ward, O. Häusser and D. L. Disdier, to be published
41) O. Häusser, A. B. McDonald, T. K. Alexander, A. J. Ferguson and R. E. Warner, Phys. Lett. submitted
42) G. H. Williams, W. E. Tucker and J. B. Ashe, ORO-2791-27 (1968) p. 114
43) F. R. Metzger, Phys. Rev. **187** (1969) 1680
44) C. Broude, Can. J. Phys. **45** (1967) 3415
45) A. E. Blaugrund, Nucl. Phys. **88** (1966) 501
46) A. Bohr and B. R. Mottelson, Mat. Fys. Medd. Dan. Vid. Selsk. **27** (1953) No. 16
47) D. C. Choudhry, Mat. Fys. Medd. Dan. Vid. Selsk. **28** (1954) No. 4
48) A. de Shalit, Phys. Rev. **122** (1961) 1530
49) N. Auerbach and N. Stein, Phys. Rev. Lett. **28B** (1969) 628
50) M. L. Rustgi, J. G. Lucas and S. N. Mukherjee, Nucl. Phys. **A117** (1968) 321
51) O. Häusser, H. J. Rose, J. S. Lopes and R. D. Gill, Phys. Lett. **22** (1966) 604;
H. J. Rose and J. S. Lopes, Phys. Lett. **22** (1966) 601
52) A. R. Poletti, E. K. Warburton and D. Kurath, Phys. Rev. **155** (1967) 1096
53) H. J. Rose, O. Häusser and E. K. Warburton, Rev. Mod. Phys. **40** (1968) 591
54) N. H. Lazar and E. D. Klema, Phys. Rev. **98** (1958) 695
55) J. Blomqvist and J. Wahlborn, Ark. Fys. **16** (1960) 545
56) A. P. Shukla and G. E. Brown, Nucl. Phys. **A112** (1968) 296
57) G. A. Beer, P. Brix, H.-G. Clerc and B. Laube, Phys. Lett. **26B** (1968) 506
58) J. A. Becker and D. H. Wilkinson, Phys. Rev. **134** (1964) B1200
59) M. Danos and E. G. Fuller, Ann. Rev. Nucl. Sci. **15** (1965) 29
60) M. Harvey and F. C. Khanna, Nucl. Phys. **A152** (1970) 588
61) H. Noya, A. Arima and H. Horie, Prog. Theor. Phys. Jap., suppl. **8** (1958) 33
62) S. Kahana, H. C. Lee and C. K. Scott, Phys. Rev. **180** (1969) 956